International Journal of Advances in Engineering and Management (IJAEM)
Volume 4, Issue 12 Dec. 2022, pp: 266-276 www.ijaem.net ISSN: 2395-5252

Offshore Cable Laying Analysis in Shallow Water Regions

OKENZE Sydney Ugochukwu, Dr. Orji Charles, Elakpa Ada Augustine

Rivers State University, Port Harcourt
Rivers State, Nigeria.
Corresponding Author: lakpa, Ada Augustine

Date of Submission: 08-12-2022 Date of Acceptance: 16-12-2022

ABSTRACT:The research is aimed at predicting the dynamic behaviour of offshore cable during installation in an S-lay configuration to ensure that the cable design criteria are met to prevent failure of the system. The analysis model is generated in Orcaflex, a non-linear time domain, finite element program which can deal with arbitrarily large deflections of submarine cable from initial configurations. In actual condition, the cable laying vessel (CLV) will respond to environmental loads due to wave, wind and current which make the CLV be in motion and reduce the operational level and affects the cable installation process. ANSYS aqwa,a radiation/diffraction program based on the main assumptions of small sinusoidal waves and vessel motions was used to obtain the CLV RAOs which is an input to the numerical analysis. Static and dynamic analysis are performed in Orcaflex over a realistic period of 3-hours simulation. The laying parameters (e.g. minimum lay angle, maximum lay tension, minimum layback) are obtained and checked with the cable operational limit criteria to verify the cable capacity in combined tension and bending with respect to radial compression from cable tensioner. Furthermore, a MathLab program was written and run to validate the result with that of Orcaflex, the result shows generally good agreement, however it should be noted that computational results depend on the accurate description of the model.

KEYWORDS: RAO, Heave, Pitch, Response,CLV, TDZ, GM.

I. INTRODUCTION

An offshore cable is an important component of the drilling facility that creates the linkage between the onshore or Upper and lower equipment. During installation, these cables usually consist of a dynamic part and a static part. The static part is installed by a cable laying ship on the seabed in corrugated environmental conditions. The dynamic parts are usually suspended so that they are not affected by the movement of the ship or the environment. A touchdown zone, the zone where the cable first touches the seabed, is necessary to account for cable failure during installation. This region can experience unacceptable bending and axial compression, resulting in localized buckling within the cross-section, making the cross-section torsionally unstable, looping globally, or both. combination can occur, ultimately leading to capacitance failure[12]. Current practice is to avoid occurrences in the touchdown zone to eliminate the possibility of cable breakage. It is often not clear how much an offshore composite submarine cable can be compressed to compromise its integrity. Cable manufacturers are often reluctant to approve substantive cables. However, the dynamic response to CLV, especially movement along the cable axis (CLV jerk), has a large impact on the axial force on the cable during installation, limiting the weather window for installation. Limited weather windows lead to high installation costs. Therefore, it is very important to study different installation scenarios and propose efficient analytical tools for cable installers to scrutinize the cable installation process with the aim of eliminating idle time in CLV.

Offshore Submarine cables can be categorized into either structural cable, signal cables or power cables depending on their application area and purpose design for. An umbilical cable combines the functionality of each of these categories, [13]The umbilical cable will when installed normally consist of both a static and dynamic part. The dynamic part of the umbilical cable is designed to hang as a catenary line from either a floating or a fixed structure. This part is subjected to high tensile loading and fatigue

International Journal of Advances in Engineering and Management (IJAEM)
Volume 4, Issue 12 Dec. 2022, pp: 266-276 www.ijaem.net ISSN: 2395-5252

mechanisms due to vessel motion. The static part is the part of the umbilical cable laying on the seabed, [16]. The design of the umbilical cable cross-section is normally governed by these verities of the loading to which the dynamic part is subjected to, as well as the requirements of the control system. Figure 2.1 shows a typical cable cross section, with named components [4].

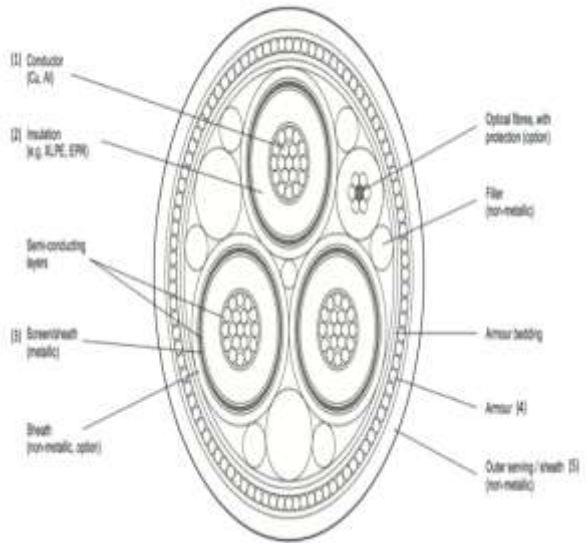

Figure 2:Tpical 3-Phase Alternating Current Power Cable cross-section

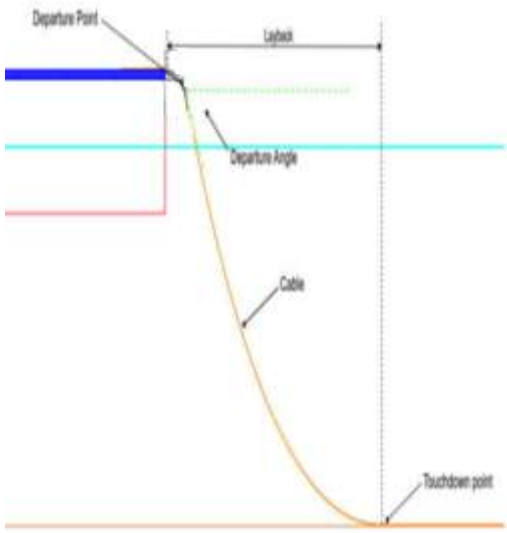

Figure 1:Cable Laying

An offshore submarine cable typically consists of: (1) a centre core of conductors; (2) an insulation system; (3) sometimes an electrical or magnetic shield; (4) a protective armour layer to protect the conductors and to provide strength; (5) an outer sheath as an outside cover, [13]

THEORICAL FORMULATIONS

This section describes the method that is used to analyse the dynamic response of the cable during installation conditions. The software used for the analysis is "Orcaflex". It is a nonlinear time-domain finite element program that can handle arbitrarily large deviations of the submarine cable from its original configuration. Lumped mass elements are used, which greatly simplifies the mathematical formulation and allows the user to include additional curses and constraints in the system according to engineering needs. The purpose of this study was to identify the operating limit criteria in the selected installation area, determine the installation parameters (minimum twist angle, maximum twist stress, minimum recoil, etc.) and combine tension and bending with respect to radial compression of the cable. To demonstrate cable bearing capacity. Contact between the machine track and the stinger roller. Departure point: Point from where the cable leaves the chute.

Loads on Lay Cable

Static loads

The cable self-weight loading can be modelled as a force per unit reference volumeF_w.

$F_w = \rho g$ (1)

An element submerged into water will be exposed to a buoyancy force equal to the weight of the displaced water, per Archimedes' law. For a cable segment with length ds the buoyancy force F_B is defined as

$\mathcal{F}_{B=} \rho g w A_e$(2)

Assuming that the cable is fully submerged, one can consider the resulting static force on the cable, named the "effective weight", to include the self-weight and the buoyancy of the cable [1]

The effective weight is also sometimes referred to as the submerged weight and can be taken as

$W_s = \mathcal{W} - \rho g w A_e$ (3)

International Journal of Advances in Engineering and Management (IJAEM)
Volume 4, Issue 12 Dec. 2022, pp: 266-276 www.ijaem.net ISSN: 2395-5252

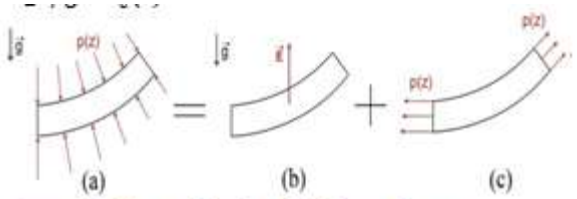

Figure 3:Effective Weight and Effective Tension Description

Dynamic Loads

The contributions from the hydrodynamic loading can be decomposed in a drag and a lift component. The lift actions of the fluid can be neglected for simplifications. To consider a mean hydrodynamic force, a common approach is to consider drag forces using Morison's model (see[9]). The magnitude of the fluid force $\mathcal{d}$F per unit length of a beam element can be written as

$$dF = \rho f \mathcal{A} \ddot{U} + Ca \rho f \mathcal{A}(\ddot{U} - \dot{u}) + \frac{1}{2}\rho f D C_d \left|\dot{U} - u\right|(U-u) \quad (3.4)$$

Where ρfis the fluid density, $\mathcal{A}$ is the dislocated fluid per unit length, Ca is the added mass coefficient, D is the external diameter of the cross-section, C_d is the drag coefficient,$\dot{U}$ is the fluid velocity magnitude and $\ddot{U}$ is the fluid acceleration magnitude. The drag forces can then be decomposed in axial (aligned with the beam axis) and orthogonal (normal to the beam axis) contributions [1], yielding.

$$DF = dF_t + dF_n \quad (5)$$

$$dFt = -C_{at}\rho f \mathcal{A} u_t + \frac{1}{2}\rho f D C_{dt} \| \dot{U}_t - \dot{u}_t \| (\dot{U}_t - \dot{u}_t) \quad (6)$$

$$dFn = -C_{an}\rho f \mathcal{A} u_n + \frac{1}{2}\rho f D C_{dn} \| \dot{U}_n - u_t \| (\dot{U}_t - \dot{u}_t) \quad (7)$$

The fluid particle velocity and acceleration are strongly dependent on the severity of the sea state. A sea state can either be represented as regular or irregular waves.

Regular Waves

A simplified representation of waves is a regular wave representation. The simplest wave theory is the Airy wave theory where the waves are represented as harmonic sinusoidal waves with linearized boundary conditions Plate 3.2. The wave surface elevation is then described as a harmonic motion at the form.

$$\eta(x,t) = \eta_0 R_{e\left[e^{i(\omega t - kx)}\right]} = \eta_{0\,cos\,(\omega t - kx)} \quad (8)$$

Where ω is the angular frequency of the wave, k is the wave number and η_0 is the wave amplitude.

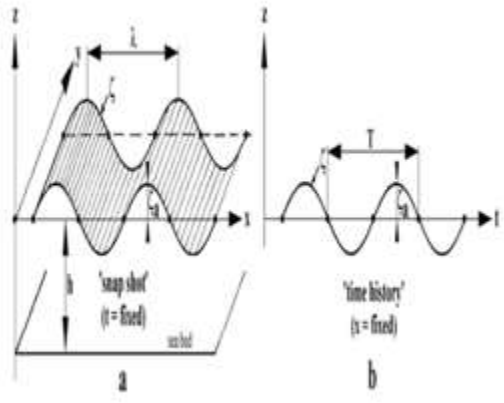

Plate 3.2: Harmonic Wave(Journee and Massie, 2001)

Irregular waves

Waves are an irregular phenomenon with natural random occurrence. Sea waves are irregular in both time and space, and the distribution of the sea surface elevation caused by waves can be modelled either in the frequency-domain or the time-domain. In the time-domain the wave train are analysed as a sequence of individual regular waves defined by two main parameters; the wave height H and the wave period T, [3].[4]. The randomness of

International Journal of Advances in Engineering and Management (IJAEM)
Volume 4, Issue 12 Dec. 2022, pp: 266-276 www.ijaem.net ISSN: 2395-5252

the sea state is captured by introducing a wave spectrum. A wave spectrum describes the distribution of wave energy as a function of wave frequencies. The spectrum is produced assuming that the sea state is stationary for a short duration of typically 3 hours.

The surface elevation is expressed as:

$$\eta = \sum_{j=1}^{N_\beta} \sum_{K=1}^{N_\beta} A_{jk\, e^{i(\emptyset k^t + e_{jk}^p + \emptyset_{jk})}} \quad (9)$$

$$A_{jk=(\sqrt{2S_\eta(\beta_{j,\omega_k})\Delta\beta\Delta\omega})} \quad (10)$$

Where A_k is the wave component amplitude given in equation (3.10), Φ_{jk} are random phase angles, which are sampled from a uniform distribution over$[-\phi, \phi]$, while Φ_{jk}^p are position dependent phase angles. The random phase angles of the wave time series are generated by defining a starting integer value called seed. Different seeds of random phase angles result in different time series, ([8],[4]). Thus, to cover the whole range of statistical waves, several different seeds need to be used.

The duration of the time series is limited to T=$N_t \Delta t \approx 2N_\omega \Delta t$. The duration T_{sim} will be adjusted to cover the duration of the dynamic analysis if necessary [14]. It exists various standardized wave spectra, where Pierson Moskowitz and JONSWAP are the most used. The two-parameter Pierson Moskowitz spectrum is defined as

$$S_\eta(\omega) = A\omega^{-5}(e^{\frac{-B}{\omega^4}}),\ 0 < \omega < \propto \quad (11)$$

$$A = 124.2\frac{H_s}{T_s^4} \quad (12)$$

$$B = \frac{496}{T_s^4} \quad (13)$$

Where T_s is the zero-up crossing frequency, which relates to the peak period with the following relation $T_{p=1.408T_s}$. The three parameter JONSWAP spectrum is given as

$$S_\eta = a g^2 \omega^{-5} e\left[-\beta\left(\frac{\omega p}{\omega}\right)\wedge 4\right]\gamma^{e\left[\frac{-(\omega-\omega)^2}{2\sigma^2\omega_p^2}\right]} \quad (14)$$

Where

$$\alpha = 1.2905\frac{H_s^2}{T_z^2} \quad (15)$$

$$\beta = \begin{cases} 1.205 & for\ North\ Sea\ Condtions \\ 1 & for\ T_p \gtrsim \sqrt[5]{H_s} \end{cases} \quad (16)$$

$$\gamma = \begin{cases} exp\left[5.75 - 1.15\frac{T_p}{\sqrt{H_s}}\right] \\ 5.0 \quad for\ T_{p<}{}^{3.6\sqrt{H_s}} \end{cases} \quad (17)$$

$$\sigma = \begin{cases} 0.07\ for\ \omega \geq \omega_p \\ 0.09\ for\ \omega \leq \omega_p \end{cases} \quad (3.18)$$

$$\omega_{p=\frac{2\pi}{T_p}} \quad (3.19)$$

$$\frac{T_p}{T_z} = 1.407(1 - 0.287ln\gamma)^{\frac{1}{4}} \quad (3.20)$$

The wave direction angle is defined relative to the global coordinate system x-axis and counterclockwise, which is shown in Plate 3.3

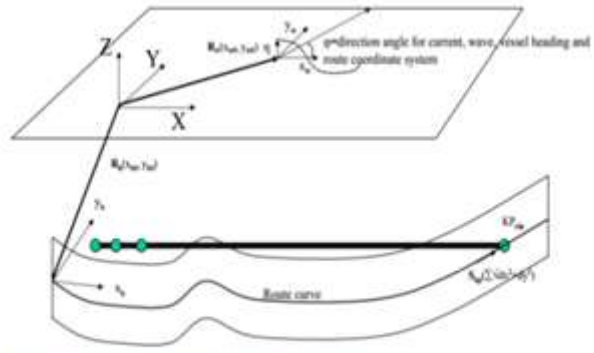

Figure 4Defination of Wave Heading

Plate 3.3: Definition of Direction Angle for Current and Waves (Saevik, 2008)

3.4 Current

The presence of current will induce drag forces on the cable. For a fixed cylinder in current along, the flow component perpendicular to the cylinder axis will induce a quadratic drag force, which can be expressed as

$$F_c = \frac{1}{2}\rho U^2 C_D\, sin.^2 K \quad (3.21)$$

where K in this context is the cone angle between velocity vector and cylinder central axis. This last sin term acknowledges the fact that a current incoming from either 90° or 270° according to Figure 2.5 will yield highest resulting force on the cable [9].

International Journal of Advances in Engineering and Management (IJAEM)
Volume 4, Issue 12 Dec. 2022, pp: 266-276 www.ijaem.net ISSN: 2395-5252

Vessel Induced Movement

During installation, the cable laying vessel will induce forced motion of the cable top connection. The cable top connection undergoes a certain time-dependent movement due to the dynamic behaviour of the container. This results in a time-dependent relative velocity between the cable and the seawater, resulting in a hydrodynamic damping force. Models can be synthesized via the Response Magnitude Operator (RAO). This allows evaluation of the movement of the floating vessel in relation to specific sea conditions.

The wave frequent motions are described by a set of complex transfer function$H_{WFJ}(\beta,\omega)$. The transfer function describes how the system responds a wave excitation with unit amplitude for various frequencies ω and wave headingθ, by describing the relation between the response and the excitation.

$$H_{WFJ(\beta,\omega)}=\frac{x_j(\beta,\omega)}{\zeta_1(\beta,\omega)} \quad (22)$$

Where $x_j(\beta,\omega)$ is the response amplitude in dof j and $\zeta_1(\beta,\omega)$ is the surface elevation amplitude[14]. The absolute value of a transfer function is known as the response amplitude operator. The RAO can be estimated using the spectral relation given in Equation (3.23) where $S_{xj}(\beta,\omega)$ and $S_\zeta(\beta,\omega)$ is the energy density spectrum of the response and the incoming wave spectrum respectively.

$$S_{xj}(\beta,\omega)=|H\_WFJ(\beta,\omega)|^{2*S_\zeta(\beta,\omega)} \quad (23)$$

The RAO translates the wave characteristics to vessel movements and are defined in all six degrees of freedom for a vessel; surge, yaw, heave, roll, pitch, sway. For laying operations, 4motion in pitch and heave have the largest in sequence on the vertical movements of the laying wheel. Roll motions will also in sequence if the laying wheel is located off the vessel's central [12]

Minimum Bending Radius

As mentioned earlier, a possible consequence of the catenary configuration is buckling and over bending due to high load accumulation at the touchdown point. A measure introduced to avoid this effect, is the minimum bending radius and associated minimum radius of curvature. The minimum bending radius denotes the minimum radius a cable can be bent at a specific load and a specific time. Bending radius below the MBR might induce cable failure, which is to be avoided to the extents possible. DNV and API operate with methods for determining the MBR, as well as presenting safety factors which shall ensure safe operation. [2] determines the MBR using the concepts of storage minimum bend radius (SR) and locking radius (LR). The standard states that the "storage minimum bend radius shall be calculated as the minimum bend radius that satisfies all the requirements of the table [2]

The bend radius required to cause locking, the locking radius, in the interlocked layers shall be calculated. The SR shall be at least 1.1 times the LR, and the MBR must not be smaller than the SR for all loading conditions.

The locking radius is found considering the bending strain needed to close the gap at the tensile or compressive sides of the cable. For interlocked poles this can be formulated as

At the compression side:

$$\frac{L_p}{n}\frac{R}{\rho\iota}=\frac{L_p}{n}-\frac{b_{min}}{\sin\alpha} \quad (24)$$

At the tensile side:

$$\frac{L_p}{n}\frac{R}{\rho\iota}=\frac{b_{min}}{\sin\alpha}-\frac{L_p}{n} \quad (25)$$

For the tensile armour layer, the compressive side applies resulting in

$$\rho\iota=\frac{R}{1-F_j} \quad (26)$$

The locking radius for the pipe is taken to be the largest $\rho\iota$for all helical layers. The integrity of the plastic layers is governed by the maximum allowable strain. This yields a limit for the bending radius of the plastic layer as given in equation (3.27). This equation also holds for the armour layers, when determining the bending radius in the case of maximum allowable bending stress.

$$\rho\iota=\frac{R}{\varepsilon lim} \quad (27)$$

The resulting bending radius is established as the value which yields the smallest radius of curvature, including safety factors as specified in [2]

Torsional Instability

The Greenhill Criterion provides an indication of the point of instability when an attempt is made to increase torque in response to an applied stress and the minimum amount of torque required to prevent looping under the amount of induced torque. Shows stress values (Ermolaeva et al., 2008). The analytical buckling criteria are for a beam of length l, the enforced displacement at both endpoints (except axially at one of the endpoints where the load is applied), the bending stiffness EI, the compressive load P and the torsional moment, Mt.

The differential equation for the beam in y- and z-direction is given in (3.28) and (3.29), where w and v are displacements in y- and z-direction, respectively. The solution of the differential equation is generally given on the form in Equation (3.30) .

$$EI\omega'' - M_t v' + P\omega = 0 \quad (28)$$

International Journal of Advances in Engineering and Management (IJAEM)
Volume 4, Issue 12 Dec. 2022, pp: 266-276 www.ijaem.net ISSN: 2395-5252

$EI\upsilon'' + M_t\omega' + P\upsilon = 0$ (29)

$\upsilon = Ae^{i\omega x}, \omega = Be^{i\omega x}$ (30)

Introducing the general solution into the differential equation yields a system of two homogeneous linear equations, which is presented in Equation (31)

$$\begin{bmatrix} P - EI\omega^2 & iM_t\omega \\ -iM_t\omega & P - EI\omega^2 \end{bmatrix} \binom{A}{B} = 0 \quad (31)$$

Deflection is possible if the determinant of the matrix is equal to zero (Bazant et al, 1991) which indicates that

$EI\omega^2 \pm M_t\omega - P = 0$ (32)

By only considering a positive torque, the solution of the equation becomes.

$\omega_{1,2} = \frac{1}{2EI}(-M_t \pm \sqrt{(M_t^2 + 4EIP)}$ (33)

$\upsilon = A_1 e^{i\omega_1 x} + A_{2e^{i\omega_2}} x$ (34)

$\omega = B_{1e^{i\omega_1 x}} + B_{2e^{i\omega_2 x}}$ (35)

Where $A_{1,}A_{2,}B_{1,}B_2$ are complex constant. Introducing the boundary constraints, the following relation between ω_1 and ω_2 are found.

$\omega_\omega = \omega_I + \frac{2\Pi}{\iota}$ (36)

Which by combining 3.36 and 3.33 yields the following expression

$\frac{\Pi}{\iota} = \frac{\sqrt{M_t^2 + 4EIP}}{2EI}$ (37)

Equation (3.37) can be rearranged, and gives the following critical load condition to cause instability Neto et al (2013),

$\frac{P}{P_{cr}^o} + \left(\frac{M_t}{M_{t,cr}^o}\right) \wedge 2 = 1$ (38)

The critical torsion moment $M_{t,cr}^o$ and critical compressive axial P_{cr}^o is given by

$P_{cr}^0 = \frac{\sqcap^2 EI}{L^2}$ (39)

$M_{t,cr}^o = \frac{\sqcap kEI}{L}$ (40)

With k=2 for the mentioned boundary conditions ([14]), Equation (40) is known as Greenhill's equation. (Liu, 1975) presented a study concerning the loop formation in electromechanical cables with single and multiple wires. Greenhill's formula is then rewritten in the case of an applied tensile load $T = -P$ which leads to Equation (41) if one considers a beam with a large length l, such that $\frac{T}{\frac{\sqcap^2 EI}{L^2}} \gg 1$.

$\frac{T}{\frac{\sqcap^2 EI}{L^2}} = \frac{M_t^2}{\left(\frac{k\sqcap EI}{L}\right)\wedge 2}$ (41)

Which also can be written as

$T = \frac{M_t^2}{k^2 EI} = \frac{M_t^2}{4EI}$ (42)

$M_t = \sqrt{4TEI}$ (43)

Based on the expression in (41), (Ross, 1977) uses energy transfer methods to evaluate the conditions of loop formation. The deduction assumes that the tension/torque conditions leading to loop formation are sustained for a long enough period for the loop to form, as well as that the cable tension is constant during loop formation. The deflection shape is assumed to be formed as a circle, while the nonlinear buckling process in real-life will lead to the formation of loops of the shape illustrated below:

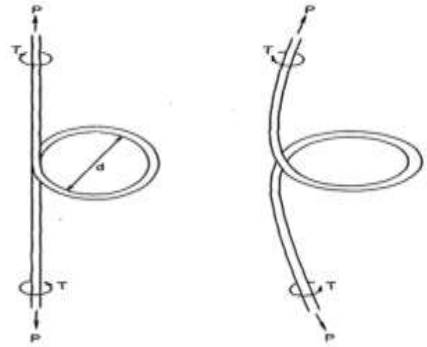

Figure 3Assumed Loop shape and Actual loop shape

Application of energy methods leads to the following relation between torque T and tension P which will lead to cable kinking.

$T = \frac{EI}{d} + \frac{Pd}{2}$ (44)

For the case of a tension-free cable, a loop of diameter d will form dependent on the value of the torsion as given in Equation (45)

$d = \frac{EI}{T}$ (45)

The loop diameter that will result in a minimum torsion to produce a loop in the elastic range is found as

$d = \sqrt{\frac{2EI}{P}}$ (46)

Substituting this equation (46) and (45) into Equation (44), yields the critical torque which will induce loop formation. The critical torque associated with loop formation is defined by Equation (47). Loop formation can be prevented if the torsion is maintained below the value defined in the equation. If the critical torsion level is exceeded, the loop formed will have a diameter as defined by the relation in Equation (48). The results found by [12] yields critical torsion moments half the size of Greenhill.

$T = \sqrt{2PEI}$ (47)

$d = \frac{\frac{2EI}{T}}{1+\sqrt{1-\frac{2PEI}{T^2}}}$ (48)

International Journal of Advances in Engineering and Management (IJAEM)
Volume 4, Issue 12 Dec. 2022, pp: 266-276 www.ijaem.net ISSN: 2395-5252

II. RESULTS

The cable installation limit can be determined with the use of the dynamic OrcaFlex models. All calculations are in accordance with the base cases defined in chapter 3. The corresponding environmental input of the cable installation analysis can be found in chapter 3. The interest in the CLV motion characteristics stems from the requirement to predict and control large-amplitude motions that can reduce the operational level and affects the performance of the process. Therefore, the prediction of the CLV motion response to waves is very important for safe operational purposes.

The installation analysis has considered the following number of cases for the various static and dynamic conditions for the submarine cable.

The total numbers of cases are given by the following.

1. Static Load – water Depth x Lay Tensions
2. Dynamic Load – water Depth x Lay Tensions x H_s x T_p x Directions.

Though, more emphasis will be lay on the dynamic load.

The tables 4.1 below present the permutations of load cases considered for general lay.

Table 4.1: Permutation of Load Cases Considered

Water Depth M	Lay Tension (KN)	H_s (m)	T_p (s)	Directions (^{0})	Currents (m/s)
21.90	2	0.75	$\sqrt{13H_s}\ s$	(0^0 – 360^0)	0 m/s
17.50	4	1.00	$\sqrt{22H_s}\ s$		0.571 m/s
22.50	6	1.25			
27.50	8	1.50	$\sqrt{32H_s}\ s$		

Compression in cables is conservatively not allowed in the analyses. The primary mode of failure is noted to be compression in the cable due to vessel motion under wave action (predominantly 60°, 120°, 240° and 300°).

To reduce the computation load, the model was subjected to 1-minute build-up period combined with 15-minutes sea state condition. To ensure the most onerous condition is captured in the simulation, the 3-hours sea state was observed, and a simulation time offset was applied to capture the identified peaks within the 3-hour sea state. Table 3.3 gives the peak waves which were identified for the sea states of 0.75m Hs up to 1.75m Hs, and the applicable time offsets which was applied for the respective sea state. The same approach was used for the higher sea states up to 2.25m Hs.

The following diagrams presented in Figure 3.1 through Figure 3.2 are the wave profile for the 3-hour sea state (left) and the corresponding 15-minute calibrated sea state (right) utilized in the simulations.

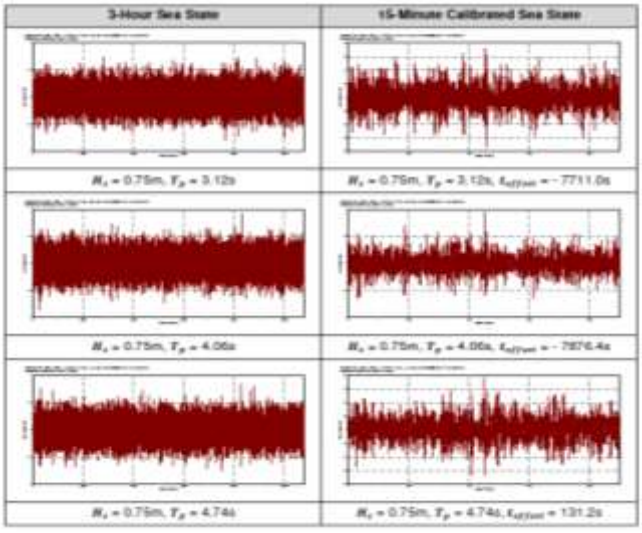

Figure – 3-Hour Sea State profile for and Hs = 0.75m @ Tp =$\sqrt{13H_s}$,$\sqrt{22H_s}$, $\sqrt{30H_s}$ and Associated Calibrated 15-Min Sea State Profile

International Journal of Advances in Engineering and Management (IJAEM)
Volume 4, Issue 12 Dec. 2022, pp: 266-276 www.ijaem.net ISSN: 2395-5252

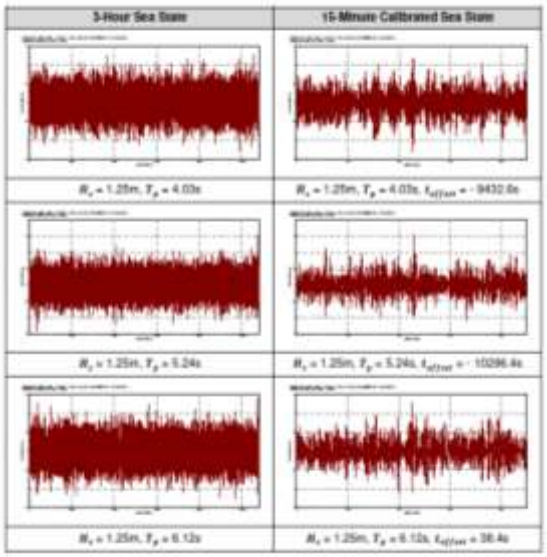

Figure – 3-Hour Sea State profile for and Hs = 1.25m @ Tp =$\sqrt{13H_s}$,$\sqrt{22H_s}$, $\sqrt{30H_s}$ and Associated Calibrated 15-Min Sea State Profile

Dynamic Load Motion Response Amplitude Operators (RAOs)

The motion response amplitude operators (RAOs) with wave heading from 0 degree to 180 degree with 30-degree interval obtained from the CLV hydrodynamic analysis in ANSYS AQWA are plotted in excel as shown below. For surge, sway, heave, roll, pitch, and yaw respectively. The predominant motion response when the CLV is subjected to following and head sea condition with the wave direction $0^o and\ 180^o$ respectively are surge, heave, and pitch motions. However, for beam sea condition the predominant responses are sway, heave and roll motions. Furthermore, there is a significant response in all six degrees of freedom when subjected to oblique sea condition.

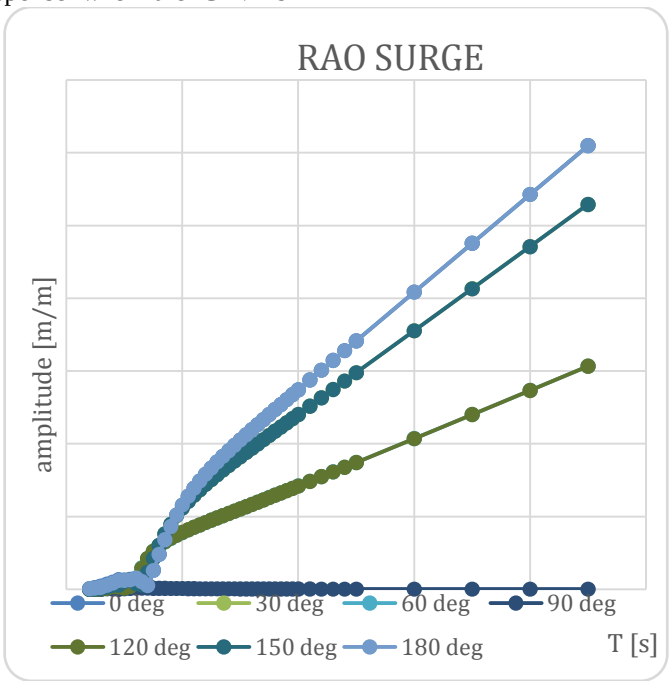

Figure :Surge RAO against Time with Varying Wave Encounter Angles

International Journal of Advances in Engineering and Management (IJAEM)
Volume 4, Issue 12 Dec. 2022, pp: 266-276 www.ijaem.net ISSN: 2395-5252

Figure 3.3 is the Surge RAO against time with varying encounter angles. The maximum RAO is observed At an encounter angle of 180^0, this is consistent with the Head Sea as the wave period increases significantly at zero and tends to maintain a constant peak value of 1 as the wave period increases. This means that the greatest vibrational disturbances are experienced at Headsea. Surges have a unique period within the displayed period range and only resonate at low wave periods.

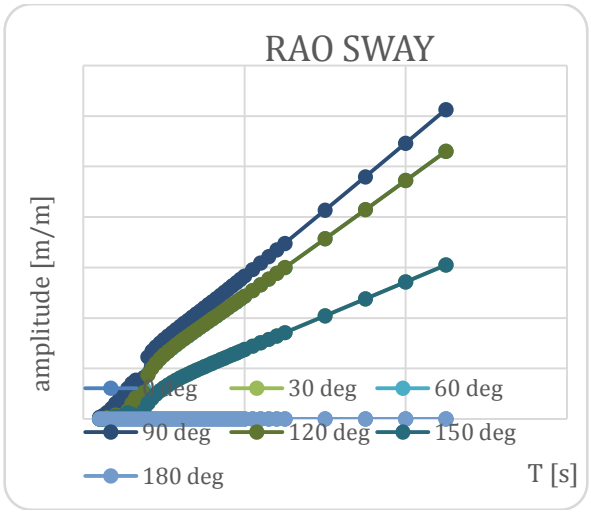

Figure :Sway RAO against Time with Varying Wave Encounter Angles

Figure 3.4 is the Sway RAO against time with varying encounter angles. The maximum Sway RAO is observed At a meeting angle of 90^0, this increases significantly from zero with the wave period, thus coinciding with the sea of rays, and tends to maintain a continuous peak of 1 as the wave period increases. This indicates that the largest disturbance of the wobbling motion occurs in Yokoumi. Reducing the hull keel reduces roll. The dominant peak of the dither response occurs at cross-sea because it increases significantly at zero wave period and tends to maintain a single constant peak as the wave period increases. However, sway affects ship handling quality more than stability.

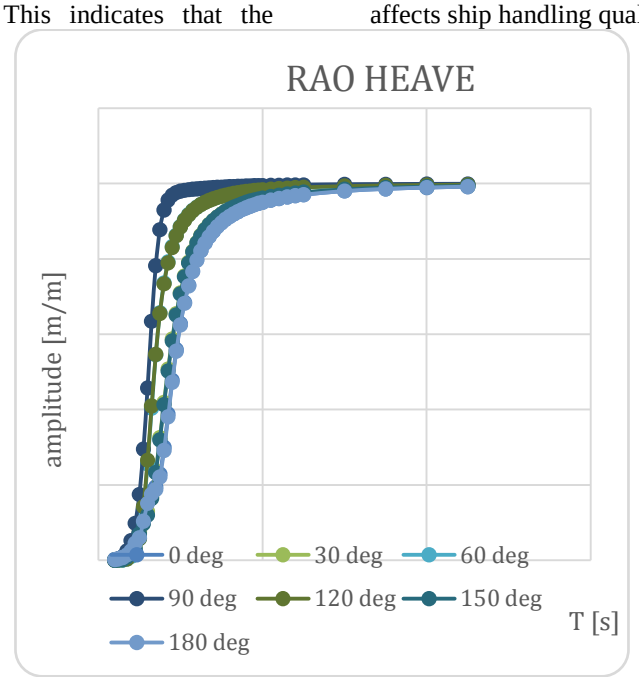

Figure:Heave RAO against Time with Varying Wave Encounter Angles

International Journal of Advances in Engineering and Management (IJAEM)
Volume 4, Issue 12 Dec. 2022, pp: 266-276 www.ijaem.net ISSN: 2395-5252

Figure 3.5 is the Heave RAO against time with varying encounter angles. The maximum Heave RAO is observed at encounter angles of 90^0 which agrees to beam sea as it increases suggestively at wave period from zero and tends to maintain a constant peak value of one as the wave period increases. This implies that, the maximum disturbance in the heave motion is experienced in the beam sea. The heave is practically well-behaved increasing from zero at short periods to one in long periods. The heave has natural period within the period range plotted and will have resonance only in low wave periods. Although the data from the analysis suggest a tendency for the peak value to move to somewhat higher dimensionless encounter frequency as the sea moves from the head sea to beam sea direction.

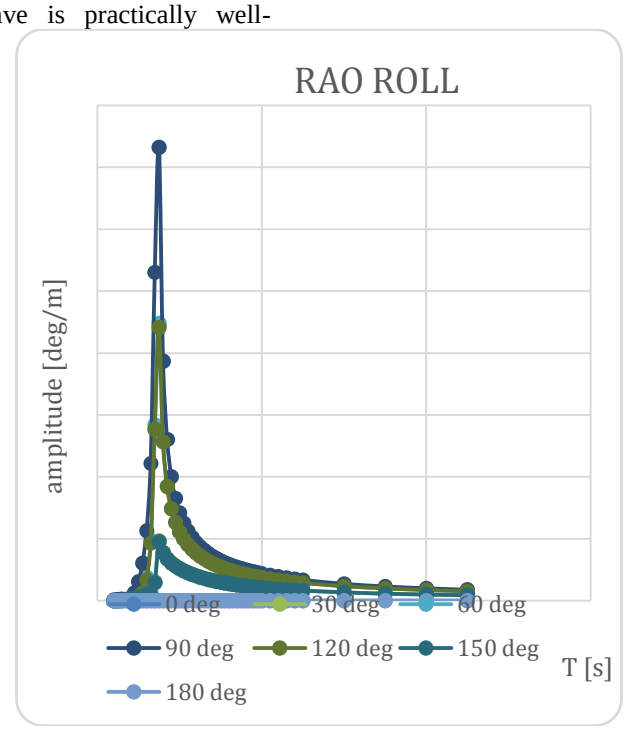

Figure:Roll RAO against Time with Varying Wave Encounter Angles

Figure 3.6 is the Roll RAO against time with varying encounter angles. The maximum Roll RAO is observed with a meeting angle of 90^0, this corresponds to a sea of bars. This is because the wave period increases suggestively at 0 and tends to maintain a constant peak value of 1 as the wave period increases. Maximum roll RAO occurs at 7.5 seconds for all encounter angles. Lateral sea rolls are the most dangerous slopes. In the sea conditions examined in this study, the maximum RAO was observed in roll motion. However, due to the CLV stability results, the Roll RAO value may result in small changes in vessel stability. Probably the best solution is to stay in a moored position and carry as much ballast as possible.

III. CONCLUSIONS

For us to determine the cable installation limit with the use of the CLV, the static lay tables are being completed with the effect of dynamic weather input as per chapter 3. The maximum significant wave height will be determined for the various wave-headings. It is not as expected that the highest cable loads are always present on the highest waves. However, simulating only a portion of the 3-hour sea state shows that the cable load is underestimated. It is concluded that the dynamics of submarine cables are governed by drag. H. Loss of cable tension is due to liquid resistance. Depending on the speed the cable reaches in the water, the weight of the cable may be supported by the tow causing free fall and loss of tension. It worth to note that, the most limiting cable integrity check is the minimum tension. According to these results, in order to not exceed the TDP distance criterion, the laying tension must not exceed 10KN.

Furthermore, the self-weight in water of the Umbilical already generates a 0.8MT tension on the tensioner, the laying tension must be slightly higher than this value to avoid any risk of falling for the umbilical. A 10KN tension is preferred as it allows keeping a ± 0.1 MT tension range during the installation. Maximum curvature, maximum and minimum tension have been checked during

calculations. Compression in cable is conservatively not allowed in the analyses. Although it is not always clear how much submarine power cables can be compressed before their integrity is compromised, cable manufacturers are often reluctant to allow significant cable compression.

The Response amplitude operator of the cable laying Vessel was analysis using ANSYS software and the results of the six degree of motion (Surge, Sway, Heave, Roll, Pitch and Yaw) of a Cable Laying Vessel (CLV) are presented with Surge RAO having a maximum value of 3.0 at 0°. Also, the Sway RAO has it maximum value of 3.0 at 90°while the Heave RAO has a maximum value of 1.0 at 0°, 90°, 120° and 150°. The Roll RAO has maximum value of 15.0 at 90° while the Pitch RAO has maximum value of 2.0 at 60° and 150° and Yaw RAO has maximum value of 0.77 at 30° and 150°.

The Response amplitude operator of the cable laying Vessel was also computed using MATLAB and the results of the six degree of motion (Surge, Sway, Heave, Roll, Pitch and Yaw) of a Cable Laying Vessel (CLV) are presented using varying heading. The 0° heading has maximum Roll RAO value of 18.0 and Surge RAO having a maximum value of 18.0. Also, the30° heading has maximum Pitch RAO value of 7.0 while 60° heading has maximum pitch value of 4.0 and the 90° heading gives maximum Heave RAO value of 4.0. the 0° heading has maximum Heave RAO value of 2.4 and the 0° heading gave a maximum Roll RAO value of 18.0.

REFERENCES

[1]. Alfredo. G. N and Clovis de Arruda Martins (2013), Structural Stability of flexible line in catenary configuration under tension. Marine Structures 34:16-40.

[2]. Elakpa,AdaAugustine,Douglas IbibaEmmanuel, Akandu Ezebuchi,DickI.F (2018),Development of preliminary ship motion prediction tool for coupled heave and pitch. American journal of Engineering Research,2018, volume 7, pp-195-204.

[3]. API. API RP 17B (2014) Recommended Practice for flexible pipe, Fifth Edition.

[4]. Elakpa Ada Augustine**,** Pullah Abeki(2022), Heave Motion Spectral a Semi-Submersible vessel Adapted for Offshore Accommodation in deep water.. International Journal of Latest Technology in Engineering, Management and Applied Science. Volume XI, Issue II

[5]. DNV (2003), DNV-OSS-032: Offshore Riser Systems.

[6]. DNV (2014). Subsea Power Cables in Shallow Water Renewable Energy Applications.

[7]. F. Rosenthal (1978): Application is Greenhill's formula to cable hockling Journal of Applied Mechanics, Transactions ASME 43(4): 681-683

[8]. J. W. Johnson, S.A Schaaf, J.R Morison, M.P Brien (1953), The force distribution exerted by surface wave in pliers.

[9]. Journee., J.M.J. Massie, W.W (2001) Offshore Hydromechanics First Edition S.I: Delft University of Technology.

[10]. Natalia S.E, Jeroen. R and Martijn P.M Krutzen (2008). Hockling behaviour of single and multiple-rope system. Engineering Failure Analysis 15(1): 142-153.

[11]. Opgard, M.F (2017). Torsion Instability of Dynamic Cables during Installation Masters' Thesis, NTNU, Trondheim, Norway

[12]. Raymond F. McAllister, J. J. Myers, and Carl H. H (1969). Handbook of ocean and S. Saevik (2015). Lecture notes in Onshore Pipeline Technology.

[13]. SveinSaevik. Simla (2008)- Theory Manual.

[14]. T.N Ohle, E. Tanttenhain , K. F. Daemrich, S. Mai (2006) Influence of spectral density distribution on wave parameters and simulation in time domain.

[15]. Torger Moan (2003), Finite Element Modelling and Analysis of Marine Structure (Prentice Hull)

[16]. Underwater engineering. McGraw-Hill Handbooks. McGraw-Hill, New York.

[17]. Worzyk. T (2009). Submarine Power Cables. Submarine Power Cables: Design, Installation, Damages and Repair, Environmental Aspects. Springer, Dordrecht.

[18]. Yong. B & Qiany. B (2005). Subsea Pipelines Risers. Mechanics of Onshore pipelines, Elsevier Science, Burlington.

[19]. Zdenerick. P. B and Luigi .C (1991), Stability of structure: elastic, inelastic, fracture and damage theories, volume 26 of the Oxford Engineering Science Series. Oxford University Press (New York).